

RoadNet-RT: High Throughput CNN Architecture and SoC Design for Real-Time Road Segmentation

Lin Bai, *Student Member, IEEE*, Yecheng Lyu, *Student Member, IEEE*, and Xinming Huang, *Senior Member, IEEE*

Abstract—In recent years, convolutional neural network has gained popularity in many engineering applications especially for computer vision. In order to achieve better performance, often more complex structures and advanced operations are incorporated into the neural networks, which results very long inference time. For time-critical tasks such as autonomous driving and virtual reality, real-time processing is fundamental. In order to reach real-time process speed, a light-weight, high-throughput CNN architecture namely RoadNet-RT is proposed for road segmentation in this paper. It achieves 90.33% MaxF score on test set of KITTI road segmentation task and 8 ms per frame when running on GTX 1080 GPU. Comparing to the state-of-the-art network, RoadNet-RT speeds up the inference time by a factor of 20 at the cost of only 6.2% accuracy loss. For hardware design optimization, several techniques such as depthwise separable convolution and non-uniform kernel size convolution are customized designed to further reduce the processing time. The proposed CNN architecture has been successfully implemented on an FPGA ZCU102 MPSoC platform that achieves the computation capability of 83.05 GOPS. The system throughput reaches 327.9 frames per second with image size 1216×176 .

Index Terms—road segmentation, real-time, FPGA, neural network.

I. INTRODUCTION

NOWADAYS autonomous vehicles have become one of the most promising technologies. Especially after the boosting development of Convolutional Neural Networks (CNNs), the perception capabilities of autonomous vehicles have been pushed into extremely high accuracy, such as vehicles or pedestrians detection [1][2], depth completion [3], road segmentation [4][5] and object tracking [6]. However, most of the high accuracy networks are very deep and have a great number of redundant parameters. Even running on the state-of-the-art GPUs, very few of them are able to work in real-time. This prevents their applications to time-critical tasks like autonomous driving. Therefore, a fast light-weight CNN with reasonable accuracy is valuable to those time-critical applications.

The road segmentation task, as one of the fundamental tasks for autonomous driving, tells the vehicles where is the possible way to drive. This task has been well-solved by a lot of researchers concerning to the accuracy. While as a time-critical task, only 3 of the existed methods are able to process in real-time (as illustrated in Fig. 1, where red line indicates the real-time boarder) and none of their throughput is higher

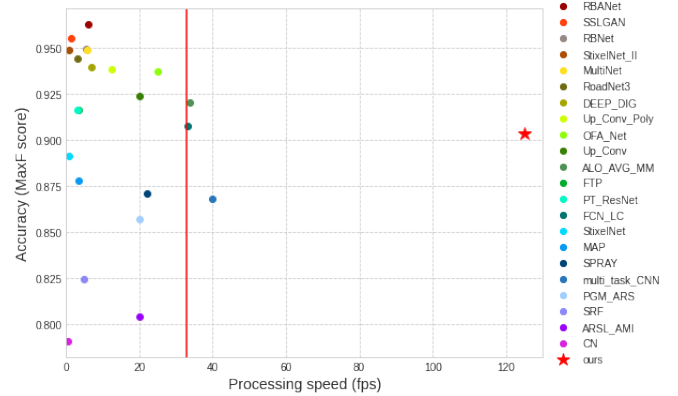


Fig. 1: Processing speed v.s. accuracy on the KITTI road segmentation test dataset. Red star indicates our method, and colored dots represent other methods. All of these solutions are tested on GPU/CPU which listed in KITTI leader-board of road segmentation task. Red line is the border of real-time.

than 40 fps. Especially, as a fundamental module prior to planning and controlling, road segmentation is expected to process one image even faster than 30 ms to guarantee the real-time response of autonomous driving systems. Thus how to segment the drivable region in a extremely short time while maintaining an acceptable accuracy is urgent to bridge the gap between the academic research and industrial practice.

In this paper, we proposed RoadNet-RT, a real-time road segmentation network, which is able to run in real-time on GPUs. Besides, we have summarized some optimization techniques aiming to convert ordinary CNN structures into hardware-friendly ones. As an example, RoadNet-RT has been implemented using these techniques and achieved real-time processing as well. The contributions of this paper are summarized as following:

- A light-weight high throughput CNN named RoadNet-RT is proposed, whose segmentation accuracy is 90.33% on KITTI road segmentation leaderboard. Through extracting features by two branches, one shallow branch for spatial information and one deep branch for context information, its inference time on NVIDIA GTX 1080 is 8 ms. When comparing to the state-of-the-art RBANet[4], this network achieves 1/20 inference time, with only 6.2% loss in accuracy.
- Considering how to convert an ordinary segmentation CNN into hardware friendly one (computation and bandwidth efficient), we make some experiments and sum-

L. Bai, Y. Lyu and X. Huang are with the Department of Electrical and Computer Engineering, Worcester Polytechnic Institute, Worcester, MA, 01609 USA e-mail: {lbai2,ylyu,xhuang}@wpi.edu.

Manuscript received

marized some guidelines quantitatively. As examples, how to employ depthwise separable convolution, how to deal with convolutions with different kernel size and dilated convolution, whether using batch normalization are analyzed.

- A corresponding hardware accelerator has been implemented on Xilinx ZCU102 MPSoC platform. By balancing the bandwidth and computation capability, this accelerator can process 83.05 Giga Operation Per Second (GOPS), equaling to 327.9 frame per second (fps).

The rest of the paper is organized as following: Sec. II summarizes the existing research on road segmentation, real-time segmentation CNNs and existing FPGA implementation for segmentation CNNs. In Sec. III, the structure of the proposed segmentation network is described together with its training details. The guidelines talking about FPGA-CNN co-optimization are placed in Sec. IV. In the following two sections, detailed hardware architecture and its performance are discussed. Sec. VII concludes the entire paper.

II. RELATED WORK

A. Road segmentation

Lots of research efforts have been paid on road segmentation task in KITTI. The RBANet proposed in [4] adopted the classical encoder-decoder structure. Instead of using the direct skip connection in U-Net [7] and SegNet [8], a residual refinement module bridged encoder and decoder parts, which consisted of reversed attention and boundary attention mechanisms. So that high resolution spatial details were preserved for decoding. Atrous Spatial Pyramid Pooling (ASPP) module was also utilized in RBANet. For images size 360×720 running on GTX Titan XP, the processing time was 0.16 second per frame. In [9], SSLGAN served to train unlabeled data and enhanced road feature representations using a discriminator from GAN. Labeled data contain many redundant areas, so training both labeled and unlabeled data prevents the overfitting problem and accelerates the convergence speed. Its processing speed was 0.7s per frame on TITAN X. A road and road boundary detection network (RBNet) was proposed in [5]. Based on a Bayesian network, RBNet could simultaneously estimate the probabilities of a pixel on the image belonging to the road and road boundary so that the road and road boundary detection were combined into a single process. It was able to process each frame in 0.18s on Tesla K20c (5 GB). StixelNet [10] posed generic static obstacles represented as stixels and learnt directly using a CNN. StixelNet II [10] was a unified network with real-time detection capability for both categorized and un-categorized objects. This network performed well on column-based obstacle detection and road segmentation but was not sensitive to the distinction of road boundaries. MultiNet [11] utilized the same encoder which was based on VGG16 to supply features to different decoders for classification, segmentation and detection tasks. In segmentation decoder, the low resolution segmentation feature map was convoluted and then upsampled using transposed convolution. It was claimed that MultiNet could perform inference at 23 fps. The structure of Up-Conv-Poly [12] was very similar to U-Net. It achieved

MaxF score 93.83%. For images with size 500×500 , this network could process each frame within 83 ms on TITAN X GPU.

Other CNN based road segmentation algorithms such as DEEP-DIG [13] and MAP [14] generated a precise drivable region but required heavy computational power.

In our previous work RoadNetV3 [15], we introduced Long-Short Term Memory (LSTM) to help finding the contour of the road. It extracted features via a FCN-like encoder. After that, several convolutional-LSTM layers followed to predict the contours of drivable region. It achieved 93.08% in accuracy but 300 ms per frame.

B. Real-time segmentation

In recent years, some researchers have shifted their focus to real-time segmentation tasks. Their solutions are generally categorized into two groups (Fig. 2), one is encoder-decoder network and the another one is multi-branch network.

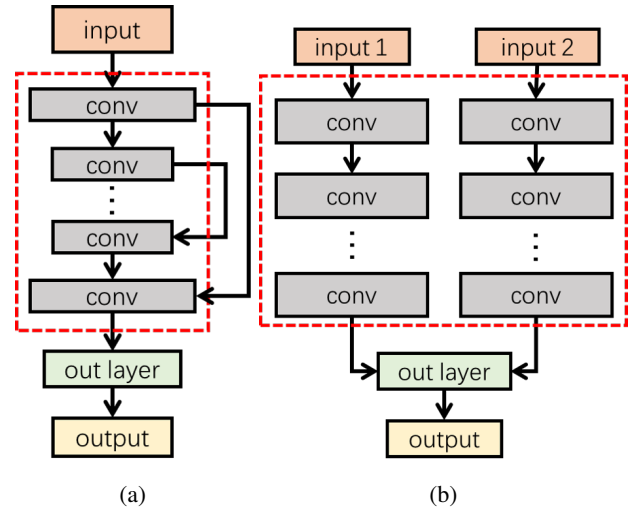


Fig. 2: The mainstream structures for real-time semantic segmentation. (a) illustrates the u-shape encoder-decoder structure and (b) demonstrates the multi-branch structure

FPENet [16] adopted the encoder-decoder structure. By using a feature pyramid encoding block to encode multi-scale contextual features with depthwise dilated convolutions in all stages and a mutual embedding upsample module as decoder, FPENet efficiently aggregated of high-level semantic features and low-level spatial details. Through introducing an efficient spatial pyramid (ESP), ESPNet [17] brought great improvement in both speed and performance. In its improved version, ESPNet-V2 [18] further enlarged the receptive field and reduced the calculation of parameters. In [19], DABNet balanced the efficiency and accuracy via stacking light-weighted blocks with different dilation rates. DFANet [20] aggregated multi-scale features from different layers to gain higher accuracy in spatial details. The light-weight backbone of DFANet guaranteed its real-time processing speed.

ContextNet [21] proposed the solution of multi-branch structure for the first time. A deep but low resolution network extracted the context information. And a shallow but

high resolution network focused on detailed spatial information. BiSeNet [22] inherited the solution of ContextNet and improved the feature fusion modules by creating attention residual module and feature fusion module. Via adding global pooling layer and residual layer, BiSeNet outperformed ContextNet. In ICNet [23], the authors borrowed the image pyramid thinking from PSPNet [24]. One more branch was added to acquire more spatial details. Plus the label guided training for each branch, ICNet had better accuracy than BiSeNet but longer processing time. BiSeNet-V2 [25] improved the first version by replacing feature fusion module into aggregation module and using Seg Head to guide the loss of each feature extractor layer. Other networks like LBN-AA [26], CANet [27] also used similar structure.

Solutions other than the two mentioned above also represent good results. FarSee-Net [28] applied Cascaded Factorized Atrous Spatial Pyramid Pooling (CF-ASPP) at the end of feature extraction layers to guarantee enough spatial information was captured. What's more, to reduce the number of operations, sub-pixel convolution was deployed, so that FarSee-Net accepted low resolution input and generated high resolution output.

C. FPGA implementation of segmentation

To accelerate the inference speed, a great amount of effort focused on FPGA implementation of segmentation neural networks. The key of hardware accelerator for CNNs was the trade-off between bandwidth and computation capability. U-Net [7] and FCN [29] are both implemented in [30]. By utilizing convolution plus board removing method, this accelerator operated transposed convolution efficiently. Its performance was 107 GOPS and supported up to 17 fps for 512×512 images. A straight-forward fully convolution neural network for segmentation has been proposed and implemented on FPGA [31][32]. Without changing the channel depth for each layer and skip connections used in U-Net [7], this accelerator pushed its performance to process 79.4 fps for input size $64 \times 180 \times 14$. Liu merged the convolution and transposed convolution into one vector multiplication unit and fused all intermediate feature maps in on-chip memory [33]. And the FPGA implementation reached 1578 GOPS, which was 57 fps for $256 \times 256 \times 3$ images. Another hardware architecture combining the convolution and transposed convolution operations was proposed in [34]. Its computation capability were 151.5 GOPS and 94.3 GOPS for convolution and transposed convolution respectively. besides, a 3D segmentation CNN accelerator was implemented in [35].

III. PROPOSED NETWORK

The proposed road segmentation network is inspired by ContextNet [21], BiSeNet [22] and ICNet [23]. It consists of two branches for context information and spatial information extraction respectively, as shown in Fig 3.

The context path is a deep network aiming to learn the context information, which consists of an input convolutional layer and two residual modules from ResNet18 [36]. After this, the extracted features are fed into ASPP layer expecting

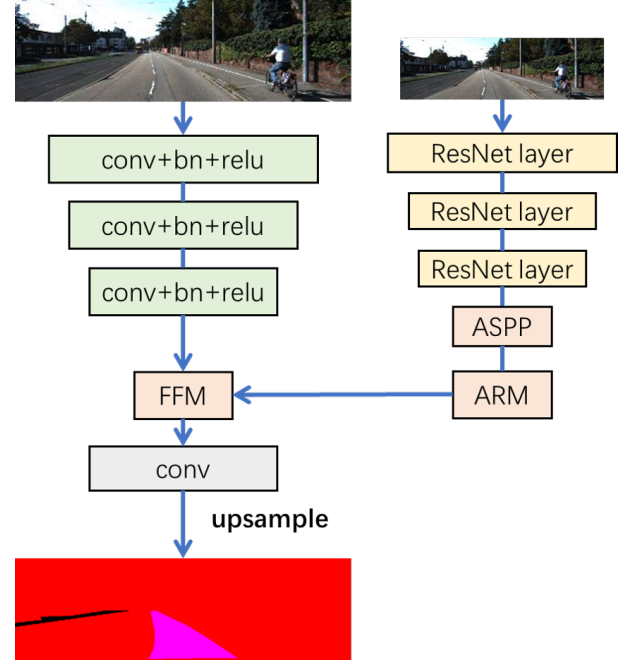


Fig. 3: Real-time road segmentation network structure

to concatenate the features from different fields of perception (dilated rates are 2, 4, 8 and 16). In the end the attention refinement module (ARM) from [22] is introduced to refine the context information. In ARM (Fig. 4a), global average pooling layer together with 1×1 convolutional layer extracts context feature and then their results refine the context features. Considering that context path does not have to focus on spatial details, therefore, to further reduce the number of operations, the input image is shrunk by a factor of 0.5 before fed into context path.

For spatial path, which focuses on spatial details of the input images, contains only three convolution layers. To enhance its capability of noticing details, no image resize is applied here. The context and spatial branches are fused in a residual refinement way, called Feature Fusion Module (FFM) [22] (Fig. 4b). The residual is the product of input feature map and its global attention path, including global average pooling layer, 1×1 convolutional layer, activation layers (ReLU and Sigmoid). At the end of the network, to reproduce the output with the same size as input, the output of FFM is upsampled 8 times by the bi-linear resize algorithm.

The number of channel is chosen to be factor of 64. This is based on the number of parallelism the hardware accelerator could support, in order to maximize the efficiency of it.

A. Training Details

This road segmentation network is implemented using Keras and trained from scratch on a single GeForce GTX 1080 GPU. All the convolutional layers were initialized using the Xavier uniform initializer [37]. During training, the batch size is set to 32. The Adam optimizer works with learning rate $1e-3$. When in plateau, a reduction rate of 0.8 is applied to the learning rate. A hybrid loss function combining Dice loss and Focal

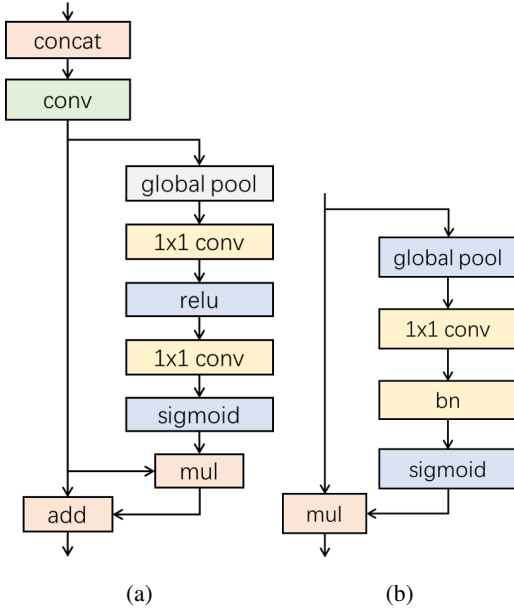


Fig. 4: (a) structure of FFM, (b) structure of ARM [22]

loss is deployed here expecting to balance the positive and negative samples.

Data augmentation for training includes random horizontal flip, Gaussian noise adding, random brightness contrast, random blurring, etc.

B. Dataset and Evaluation

The dataset for training and evaluation is the KITTI road segmentation dataset, which contains 289 training images and 290 testing images. The training image size ranges from 370×1224 to 375×1242 . The evaluation job is done by an on-line evaluation server supplied by KITTI. The evaluation (Tab.I is divided into Urban Unmarked (UU), Urban Marked (UM) and Urban Multiple Marked lanes (UMM). URBAN_ROAD is the comprehensive evaluation of the above three.

Concerning to the speed, if running on GeForce GTX 1080 GPU, this network could process each image (1216×176) within 8 ms. Four samples of predictions are demonstrated in front view and bird eye view by Fig. 5 and Fig. 6 respectively,

where green area represents the overlap between prediction and ground truth, red area is road in ground truth but not correctly predicted by our network, and blue area is not road but recognized as road by our network.

IV. NETWORK OPTIMIZATION FOR HARDWARE

In this section, we summarize some guidelines to optimize specific CNNs toward FPGAs accelerator implementation. So that on-chip resources efficiency and computation efficiency FPGA design are maximized. Different from the conventional optimization techniques, the goal of this step is to balance the number of operations, number of weights and computation patterns, while remaining the accuracy within a reasonable range.

A. Depthwise Separable Convolution

Depthwise separable convolution is initially introduced in [38]. And it has been widely adopted to a great number of light weighted neural networks such as Xception [39], MobileNet series [40][41]. The main idea of depthwise separable convolution is to decompose standard convolution into a 3×3 depthwise convolution and a 1×1 pointwise convolution to achieve less number of weights and consequently less operations. Fig. 7 illustrates how the depthwise separable convolution works, where D_K is the size of convolution kernel, M is the depth of input feature maps and N is the number of convolution kernels (also the channel number of output feature maps).

During depthwise convolution, a single filter is applied to each input channel. And then the pointwise convolution applies a 1×1 convolution to combine the outputs of the depthwise convolution. The number of weights required by standard convolution and depthwise separable convolution are calculated in (1) and (2) respectively.

$$D_K \cdot D_K \cdot M \cdot N \quad (1)$$

$$D_K \cdot D_K \cdot M + M \cdot N \quad (2)$$

Therefore, when replacing standard convolution with depthwise separable convolution, the reduction ratio of weights is

$$\frac{D_K \cdot D_K \cdot M + M \cdot N}{D_K \cdot D_K \cdot M \cdot N} = \frac{1}{N} + \frac{1}{D_K^2} \quad (3)$$

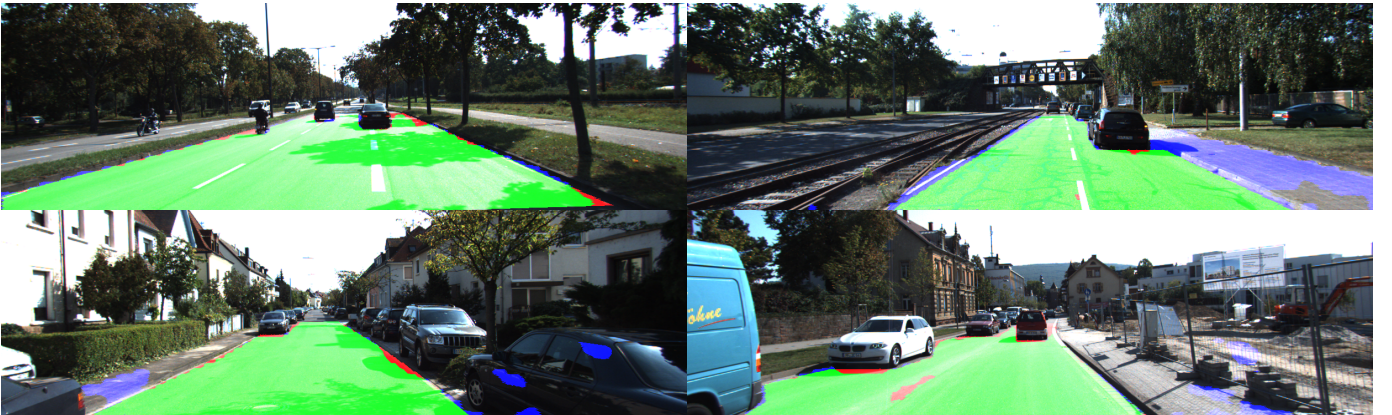


Fig. 5: Road segmentation results in camera view

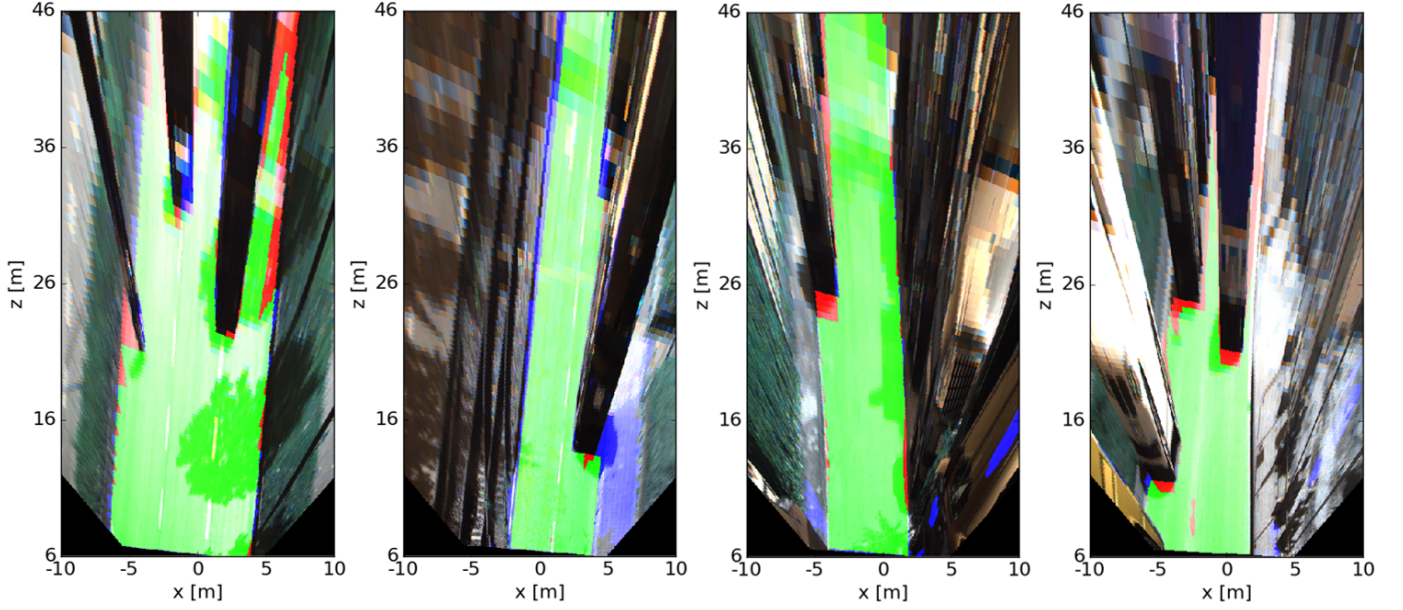


Fig. 6: Road segmentation results in Bird-Eye View

TABLE I: Performance evaluation from KITTI online test server

Benchmark	MaxF	AP	PRE	REC	FPR	FNR
UM_ROAD	88.16 %	90.24 %	87.67 %	88.65 %	5.68 %	11.35 %
UMM_ROAD	93.04 %	94.20 %	92.16 %	93.94 %	8.78 %	6.06 %
UU_ROAD	88.21 %	89.61 %	87.73 %	88.70 %	4.04 %	11.30 %
URBAN_ROAD	90.33 %	91.63 %	89.55 %	91.13 %	5.86 %	8.87 %

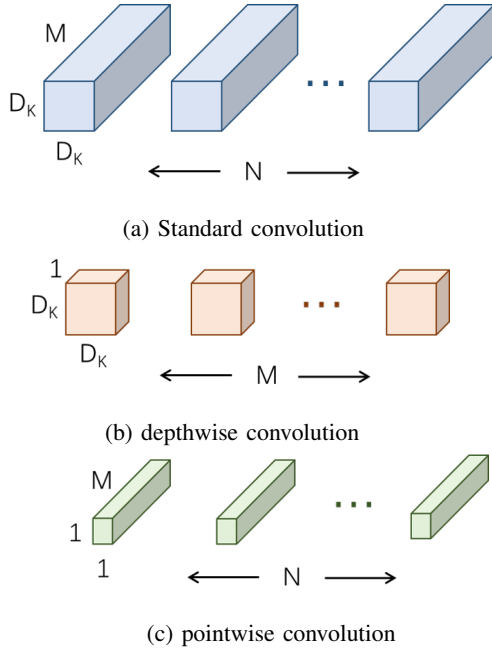


Fig. 7: The comparison between standard convolution in (a) and depthwise separable convolution with depthwise part in (b) and pointwise part in (c)

Besides the parameter reduction and operation number decreasing, from the hardware implementation point of view, depthwise separable convolution need not as large size accumulator as required by standard convolution. In standard convolution, every element of output feature map is the sum of $D_K \cdot D_K \cdot M$ elements. While in depthwise separable convolution, that is the sum of $D_K \cdot D_K$ and M elements for depthwise convolution and pointwise convolution respectively. Less bit-width accumulator leads to less critical paths and consequently increases the running clock frequency of FPGA.

Applying this to RoadNet-RT proposed in this paper, the total number of parameters is reduced from 89.93% to 87.63%, which is illustrated in Tab. II. Although the accuracy loss is 2.3%, the number of parameters reduces by a factor of 5.64.

TABLE II: Comparison of RoadNet-RT with and without depthwise separable convolution

Convolution type	IOU ¹	parameters
Standard	89.93%	756,032
Depthwise separable	87.63%	133,870

¹Since KITTI online test sever limits the submission to be 3 times per month, therefore 20% of the training set has been split as validation set to evaluate the methods we proposed. Here we choose IOU as the main metric to estimate the performance of different methods. IOU is one of the most important and the most widely used metrics for segmentation performance evaluation.

B. Large kernel size convolution

The most commonly used kernel size for convolution is 3×3 . However, in order to have large size of field of perception, especially in the first layer, large kernel size is usually desired (7×7 in ResNet[36] for instance).

Algorithm 1 Cascaded loop of standard convolution

```

for no in Nof do                                ▷ output channel, loop-4
  for (y,x) in (Noy,Nox) do                      ▷ feature map, loop-3
    for ni in Nif do                              ▷ input channel, loop-2
      for (ky,kx) in (K,K) do                    ▷ kernel, loop-1
         $F_{out}[no,y,x] +=$ 
           $F_{in}[ni,y-ky,x-kx] * K[no,ni,ky,kx]$ 
         $F_{out} += bias[no]$ 

```

However, to deal with different kernel size filters affects either parallelism of processing or the efficiency of buffer usage. From matrix multiplication point of view (in Alg. 1), through keeping the loop-1, hardware accelerator can handle different size of filters without extra multipliers consumed. But the penalty is the parallelism of loop-1 loss. However, different size of filter requires different size of on-chip memory. Consider a feature map with size $W \cdot H \cdot C$, to buffer it for $K \cdot K$ filter, memory size $(W+K-1) \cdot (H+K-1) \cdot C$ is need. So that the feature map buffer for 7×7 filter is $4 \cdot (W+H+4)/(W \cdot H)$ times larger than that for 3×3 filter.

To pursue the same perceptive field of 7×7 , three cascaded convolutional layers with kernel size 3×3 can replace one convolutional layer with kernel size 7×7 . If so, there is no extra resource needed including both multipliers and memory. Besides, the number of operations decreases. As illustrated in Fig. 8, for input feature map size $W \cdot H \cdot C_i$ and output feature map size $W \cdot H \cdot C_o$, if 7×7 filter is applied, totally $(W \cdot H \cdot 7 \cdot 7 \times C_i \cdot C_o) = 49 \cdot W \cdot H \cdot C_i \cdot C_o$ GOPS costs. In case of three 3×3 convolutional layers, $3 \cdot (W \cdot H \cdot 3 \cdot 3 \cdot C_i \cdot C_o) = 27 \cdot W \cdot H \cdot C_i \cdot C_o$.

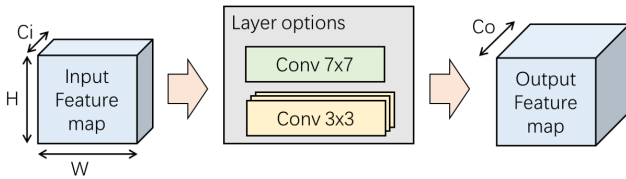


Fig. 8: Strategy for large convolutional layer replacement

The performance comparison between these two options mentioned above is shown in Tab. III. When replacing the first convolutional layer (7×7) with three 3×3 convolutional layers, the accuracy loss in IOU is 0.19%. Since there is only one layer of 7×7 convolution, the save in operations and parameters are negligible.

In the segmentation networks, dilated convolution [42] is the most widely used method to enlarge the perceptive field without introducing more weights. Unfortunately, during convolution with dilated kernel (3×3 with dilated rate equals 3 for instance), the region required from feature map is still 7×7 . This will introduce the dilemma described above still. The only

TABLE III: Comparison between 7×7 convolution and its replacement (C_i is the input feature map channel number and C_o is the output feature map channel number, they equal 32 and 64 respectively in this experiment)

Method	IOU	parameter
1 conv 7×7	89.93%	$7 \cdot 7 \cdot C_i \cdot C_o$
3 conv 3×3	89.74%	$3 \cdot 3 \cdot C_i \cdot C_o + 3 \cdot 3 \cdot C_o \cdot C_o + 3 \cdot 3 \cdot C_o \cdot C_o$

difference is, if using three 3×3 convolutional layers instead of one dilated 3×3 convolutional layers with dilated rate as 3, two times more weights and two times more operations are unavoidable. However, since the dilated convolutional layer usually won't dominant, this penalty is still affordable.

TABLE IV: Performance comparison between dilated convolution (3×3 with dilated rate 3) and its replacement

Method	IOU	parameter
1 conv 3×3 dilated rate 3	89.93%	$3 \cdot 3 \cdot C_i \cdot C_o$
3 conv 3×3	89.78%	$3 \cdot 3 \cdot C_i \cdot C_o + 3 \cdot 3 \cdot C_o \cdot C_o + 3 \cdot 3 \cdot C_o \cdot C_o$

C. Consideration of channel depth

In our hardware implementation, after considering the given resources on ZCU102 board, loop-2 in Alg. 1 has been unrolled with 32 feature maps processed in parallel. To maximum the computation efficiency of accelerator, it's better that the input feature map depth of all layers align to integer factor of 32.

D. Batch Normalization

During inference, Batch Normalization (BN) is downgraded into 1×1 convolution and further merged into convolutional layer prior than it. The merged weights and bias follow (4) and (5), where W and b represent weights and bias respectively.

$$W_{merge} = W_{BN} \cdot W_{conv} \quad (4)$$

$$W_{merge} = W_{BN} \cdot b_{conv} + b_{BN} \quad (5)$$

Batch normalization layer is helpful for fast convergence but not always a necessary layer concerning to the accuracy (PointNet[43] for instance). The contribution of BN layer is evaluated in Tab.V, from which we find in our segmentation neural network, BN helps to increase the accuracy by 1.05% without too much difference in convergence. Therefore, BN layers are kept in RoadNet-RT.

TABLE V: The performance comparison with and without BN layer, both of them are trained using the same batch size and the sam GPU

Method	with BN	without BN
IOU	89.93%	88.88%
converge@epoch	350	344
duration/epoch	9s	5s

Some experiments declared that BN after ReLU usually shows better result [44]. But this may vary from one network to another.

E. Quantization

To maximize the computation capability of FPGA, fixed point operations is preferred. Quantization aware training has been performed for 8-bit and 16-bit respectively with the help of model optimization library from QKeras[45]. Brute-force quantization may lead to unacceptable precision loss. While quantization aware training restrict the bit-width during training. This not only compensates the precision loss but introduces more non-linearity.

The performance after quantization is shown in Tab. VI. We found the accuracy (IOU) of 8-bit is 86.85%, while that of 16-bit quantization is 87.08%. The accuracy of 16-bit quantization has 0.23% higher than that of 8-bit quantization, but we list the considerations when choosing which one to implement on hardware, 1) from storage perspective, memory space for 8-bit weights is only half of that for 16-bit quantization, 2) from hardware resources perspective, each DSP48E2 core could perform two 8-bit multiplications simultaneously but only one for 16-bit multiplication [46].

TABLE VI: Performance of 8-bit and 16-bit quantized networks

Bit Width	IOU	size of parameters
8-bit	86.85%	0.127MB
16-bit	87.08%	0.255MB

V. SYSTEM-ON-CHIP IMPLEMENTATION

To fully utilize the computation resources, the whole system is partitioned into software part (done by ARM processor) and hardware part (running on FPGA). The software part job is image resize for both input and output of neural network (Fig. 3). With the help of OpenCV library [47], image resize can be easily done on PYNQ platform.

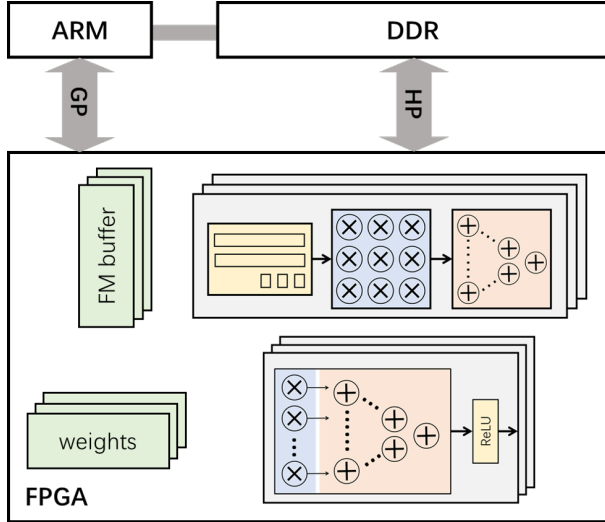


Fig. 9: Strategy for large convolutional layer replacement

The overview of hardware architecture is demonstrated in Fig. 9. It consists of depthwise convolution module, and pointwise convolution module, feature map buffers, weights buffers. A finite state machine controls the running order

of CNN operations. All the modules mentioned above are configurable based on the on-chip resources available on the target FPGA platform.

A. Depthwise convolution module

Depthwise convolution module contains line buffers, process engines (PEs) and adder trees. As described in the previous section, to unroll the kernel loop (loop-1 in Alg. 1), line buffer is needed to generate the sliding patch. Since kernel size of all the convolutional layers in this segmentation network is 3×3 , a multiplier array with length=9 follows the line buffer. Correspondingly, an adder tree in the end sums the products up. To balance the computation efficiency and on-chip resources, the batch size of depthwise convolution module is set to 32.

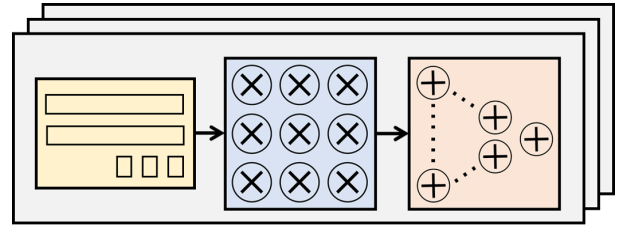


Fig. 10: Block diagram of depthwise convolution module

B. Pointwise convolution module

To align to the depthwise convolution module to fit the same size of feature buffers, the pointwise convolution module is designed to handle 32×1 vector - 32×32 matrix multiplication. There are 3 components multiplier array, adder tree, and ReLU module form the Pointwise convolution module. If the batch normalization layer is placed before ReLU layer, it can be merged and completed by multiplier array and adder tree. Otherwise, 1 extra multiplier and 1 extra adder is necessary to perform the batch normalization operation.

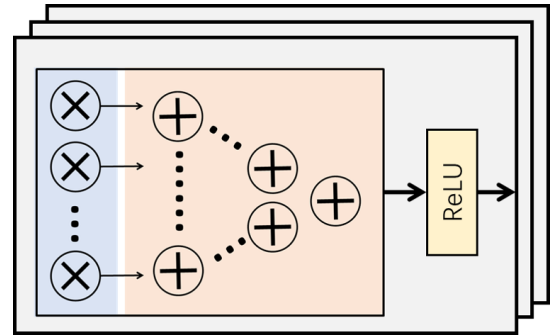


Fig. 11: Block diagram of pointwise convolution module

C. ARM Module and FFM Module

Both ARM and FFM modules require operations with totally different computation patterns. Global average pooling is to calculate the average value of one entire channel. Therefore,

an accumulator plus one multiplier for each channel has been implemented. The following 1×1 convolution is mathematically vector-matrix multiplication, which can be either routed into pointwise convolutional module or implemented with extra resource, given the resource consumption of this operation is small. Sigmoid function is approximated by the piece-wise function and implemented using a Look-Up Table.

D. Buffers

The on-chip memory are divided into buffers for feature maps, weights and global pooling result respectively. In this design, 1) there is no biases, so that no extra buffer is needed for bias storage, and 2) since the weights occupy only small portion of the on-chip memory, so that they can be hard coded into on-chip memory.

To boost the processing speed, one effective way is to reduce the number of time data transmission (between FPGA and DDR memory). Multiple feature map buffers with size $22 \times 152 \times 32$ have been implemented as ping-pong buffers to decrease data swap as much as possible.

E. Tasks on ARM Processor

Referring to Fig. 9, the entire CNN is implemented on FPGA side. The left task is images resize at the input and output of CNN respectively. Two threads of ARM processor are utilized to do input image resize and output image resize respectively.

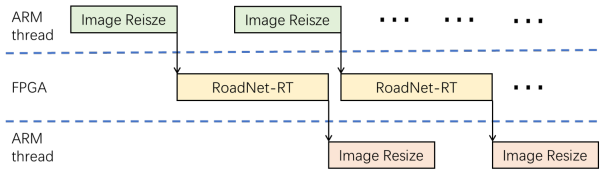


Fig. 12: Strategy for large convolutional layer replacement

VI. RESULTS AND DISCUSSION

The implementation tools used in this paper are Xilinx Vivado HLS and MATLAB HDL Coder Toolbox. The whole system has been implemented on ZCU102 development kit, with the PYNQ system installed (The system setup is show in Fig. 13). There are 548,160 Flip-Flops (FFs), 274,080 Look-Up Tables (LUTs), 1824 (32.1 Mb) Block RAMs (BRAMs) and 2,520 DSPs on the board. The FPGA resources consumption of this accelerator for both 16-bit and 8-bit quantization formats are shown in Tab. VII.

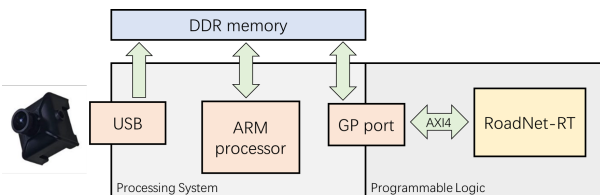


Fig. 13: Setup of road segmentation system

TABLE VII: FPGA on-chip resource usage of the road segmentation network

bitwidth	FF	LUT	DSP	BRAM
8-bit	113067	257204	1560	1057
16-bit	115158	260616	1560	1222

Since each DSP48E2 slice can handle two 8-bit \times 8-bit multiplication while the number for 16-bit number is one, thus 8-bit format accelerator consumes almost the same DSP slices and BRAMs as that in 16-bit format but twice the number of input images. When running at 200 MHz, this 16-bit version accelerator is capable to process 327.9 fps. In case of 8-bit, the processing speed is doubled to 655.8 fps. In Tab. VIII, all the image-based road segmentation solutions in the KITTI leader-board are summarized and compared to our solution in GPU and FPGA. Most of the existing methods cost 100 ms or longer. One of the only two real-time solutions FCN-LC [48] runs on TITAN X GPU, which requires 600-650W power supply on PC to support. Therefore, our solutions supply a well-balanced and practical way to run this the road segmentation task on embedded devices.

In this accelerator (16-bit version for instance), there are 8 feature map buffers are allocated. But this number may vary according to the balance between available resources on the target platform and required processing speed. More feature map buffers can store more intermediate feature maps and consequently increase the processing speed. While less feature map buffers require more temporary data stored in external memory rather than on-chip ones. And thus leads to longer processing time.

VII. CONCLUSION

This paper presents a real-time, high-throughput convolutional neural network architecture for road segmentation. Several optimization techniques are applied to reduce the number of operations while preserving the accuracy performance. This networks achieves 90.33% F1 score with 125 fps on GTX 1080 GPU (for image size 1216×176). More importantly, using RoadNet-RT as an example, we present a systematic approach on how to perform network optimization for hardware implementation. Following this as a guideline, one can easily convert any existing network structure into an computation efficient, high-through architecture for FPGA with little or none accuracy loss. Several experiments have been conducted to support the proposed approach. In the end, a SoC design has been successfully demonstrated on ZCU102 development kit, which achieves a speeds up of the processing time saving by a factor of 2.6 comparing to its GPU implementation.

REFERENCES

- [1] X. Du, M. H. Ang, S. Karaman, and D. Rus, "A general pipeline for 3d detection of vehicles," in *2018 IEEE International Conference on Robotics and Automation (ICRA)*. IEEE, 2018, pp. 3194–3200.
- [2] Z. Yang, Y. Sun, S. Liu, X. Shen, and J. Jia, "Std: Sparse-to-dense 3d object detector for point cloud," in *Proceedings of the IEEE International Conference on Computer Vision*, 2019, pp. 1951–1960.

TABLE VIII: Performance comparison of all the image-based road segmentation solutions in the KITTI leaderboard (blank means it is not mentioned in the original paper)

Name	CNN-based	Input shape	Devices	Accuracy(MaxF)	Processing speed
RBANet[4]	✓	360 × 720	TITAN XP	96.30%	160 ms
SSLGAN[9]	✓	375 × 1242	TITAN X	95.53%	700 ms
RBNet[5]	✓	300 × 900	Tesla K20c	94.97%	180 ms
StixelNet-II[10]	✓	800 × 370	Quadro M6000	94.88%	1200 ms
MultiNet[11]	✓	1248 × 384		94.88%	170 ms
RoadNet3[15]	✓	600 × 160 × 5	GTX 950M	94.44%	300 ms
DEEP-DIG[13]	✓		Titan X	93.98%	140 ms
Up-Conv-Poly[12]	✓	500 × 500	TITAN X	93.83%	83 ms
OFA-Net[49]	✓			93.74%	40 ms
Up-Conv[12]	✓	300 × 300	GTX TITAN X	92.39%	52.2 ms
ALO-AVG-MM[50]	✓	624 × 192	GTX 1080	92.03%	29.6 ms
FTP[14]	✓			91.61%	280 ms
PT-ResNet[51]	✓		GTX 1080 Ti	91.61%	300 ms
FCN-LC[48]	✓	621 × 187	TITAN X	90.79%	30 ms
StixelNet[52]	✓	24 × 370		89.12%	1000 ms
MAP[14]	✓			87.80%	280 ms
SPRAY[53]	✓	800 × 600	GTX 580	87.09%	45 ms
multi-task CNN[54]	✓	375 × 1242	unknown type GPU	86.81%	25.1 ms
PGM-ARS[55]	✓	~ 75 × 248	Intel i7-4700MQ processor	85.69%	50 ms
SRF[56]	✗	500 × 250		82.44%	200 ms
ARSL-AMI[57]	✗			80.36%	50 ms
CN[58]	✗			79.02%	2000 ms
Ours (floating point)	✓	176 × 1216	GTX 1080	90.33%	8 ms

- [3] X. Cheng, P. Wang, C. Guan, and R. Yang, “Cspn++: Learning context and resource aware convolutional spatial propagation networks for depth completion,” *arXiv preprint arXiv:1911.05377*, 2019.
- [4] J.-Y. Sun, S.-W. Kim, S.-W. Lee, Y.-W. Kim, and S.-J. Ko, “Reverse and boundary attention network for road segmentation,” in *Proceedings of the IEEE International Conference on Computer Vision Workshops*, 2019, pp. 0–0.
- [5] Z. Chen and Z. Chen, “Rbnet: A deep neural network for unified road and road boundary detection,” in *International Conference on Neural Information Processing*. Springer, 2017, pp. 677–687.
- [6] W. Choi, “Near-online multi-target tracking with aggregated local flow descriptor,” in *Proceedings of the IEEE international conference on computer vision*, 2015, pp. 3029–3037.
- [7] O. Ronneberger, P. Fischer, and T. Brox, “U-net: Convolutional networks for biomedical image segmentation,” in *International Conference on Medical image computing and computer-assisted intervention*. Springer, 2015, pp. 234–241.
- [8] V. Badrinarayanan, A. Kendall, and R. Cipolla, “Segnet: A deep convolutional encoder-decoder architecture for image segmentation,” *IEEE transactions on pattern analysis and machine intelligence*, vol. 39, no. 12, pp. 2481–2495, 2017.
- [9] X. Han, J. Lu, C. Zhao, S. You, and H. Li, “Semisupervised and weakly supervised road detection based on generative adversarial networks,” *IEEE Signal Processing Letters*, vol. 25, no. 4, pp. 551–555, 2018.
- [10] N. Garnett, S. Silberstein, S. Oron, E. Fetaya, U. Verner, A. Ayash, V. Goldner, R. Cohen, K. Horn, and D. Levi, “Real-time category-based and general obstacle detection for autonomous driving,” in *Proceedings of the IEEE International Conference on Computer Vision*, 2017, pp. 198–205.
- [11] M. Teichmann, M. Weber, M. Zoellner, R. Cipolla, and R. Urtasun, “Multinet: Real-time joint semantic reasoning for autonomous driving,” in *2018 IEEE Intelligent Vehicles Symposium (IV)*. IEEE, 2018, pp. 1013–1020.
- [12] O. G. Leivas, W. Burgard, and T. Brox, “Efficient deep methods for monocular road segmentation,” in *IEEE/RSJ International Conference on Intelligent Robots and Systems (IROS 2016)*, 2016.
- [13] J. Munoz-Bulnes, C. Fernandez, I. Parra, D. Fernández-Llorca, and M. A. Sotelo, “Deep fully convolutional networks with random data augmentation for enhanced generalization in road detection,” in *2017 IEEE 20th International Conference on Intelligent Transportation Systems (ITSC)*. IEEE, 2017, pp. 366–371.
- [14] A. Laddha, M. K. Kocamaz, L. E. Navarro-Serment, and M. Hebert, “Map-supervised road detection,” in *2016 IEEE Intelligent Vehicles Symposium (IV)*. IEEE, 2016, pp. 118–123.
- [15] Y. Lyu, L. Bai, and X. Huang, “Road segmentation using cnn and distributed lstm,” in *2019 IEEE International Symposium on Circuits and Systems (ISCAS)*. IEEE, 2019, pp. 1–5.
- [16] M. Liu and H. Yin, “Feature pyramid encoding network for real-time semantic segmentation,” in *British Machine Vision Conference 2018, BMVC*, 2019.
- [17] S. Mehta, M. Rastegari, A. Caspi, L. Shapiro, and H. Hajishirzi, “Espnet: Efficient spatial pyramid of dilated convolutions for semantic segmentation,” in *Proceedings of the european conference on computer vision (ECCV)*, 2018, pp. 552–568.
- [18] S. Mehta, M. Rastegari, L. Shapiro, and H. Hajishirzi, “Espnetv2: A light-weight, power efficient, and general purpose convolutional neural network,” in *Proceedings of the IEEE Conference on Computer Vision and Pattern Recognition*, 2019, pp. 9190–9200.
- [19] G. Li and J. Kim, “Dabnet: Depth-wise asymmetric bottleneck for real-time semantic segmentation,” in *British Machine Vision Conference 2018, BMVC*, 2019.
- [20] H. Li, P. Xiong, H. Fan, and J. Sun, “Dfanet: Deep feature aggregation for real-time semantic segmentation,” in *Proceedings of the IEEE Conference on Computer Vision and Pattern Recognition*, 2019, pp. 9522–9531.
- [21] R. P. K. Poudel, U. Bonde, S. Liwicki, and C. Zach, “Contextnet: Exploring context and detail for semantic segmentation in real-time,” in *British Machine Vision Conference 2018, BMVC*, 2018, p. 146.
- [22] C. Yu, J. Wang, C. Peng, C. Gao, G. Yu, and N. Sang, “Bisenet: Bilateral segmentation network for real-time semantic segmentation,” in *Proceedings of the European conference on computer vision (ECCV)*, 2018, pp. 325–341.
- [23] H. Zhao, X. Qi, X. Shen, J. Shi, and J. Jia, “Icnet for real-time semantic segmentation on high-resolution images,” in *Proceedings of the European Conference on Computer Vision (ECCV)*, 2018, pp. 405–420.
- [24] H. Zhao, J. Shi, X. Qi, X. Wang, and J. Jia, “Pyramid scene parsing network,” in *Proceedings of the IEEE conference on computer vision and pattern recognition*, 2017, pp. 2881–2890.
- [25] C. Yu, C. Gao, J. Wang, G. Yu, C. Shen, and N. Sang, “Bisenet v2: Bilateral network with guided aggregation for real-time semantic segmentation,” *arXiv preprint arXiv:2004.02147*, 2020.
- [26] G. Dong, Y. Yan, C. Shen, and H. Wang, “Real-time high-performance semantic image segmentation of urban street scenes,” *IEEE Transactions on Intelligent Transportation Systems*, pp. 1–17, 2020.
- [27] Q. Tang, F. Liu, J. Jiang, and Y. Zhang, “Attention-guided chained context aggregation for semantic segmentation,” *arXiv preprint arXiv:2002.12041*, 2020.
- [28] Z. Zhang and K. Zhang, “Farsee-net: Real-time semantic segmentation by efficient multi-scale context aggregation and feature space super-resolution,” *arXiv*, pp. arXiv–2003, 2020.
- [29] J. Long, E. Shelhamer, and T. Darrell, “Fully convolutional networks

- for semantic segmentation,” in *Proceedings of the IEEE conference on computer vision and pattern recognition*, 2015, pp. 3431–3440.
- [30] S. Liu, H. Fan, X. Niu, H.-c. Ng, Y. Chu, and W. Luk, “Optimizing cnn-based segmentation with deeply customized convolutional and deconvolutional architectures on fpga,” *ACM Transactions on Reconfigurable Technology and Systems (TRETS)*, vol. 11, no. 3, pp. 1–22, 2018.
- [31] Y. Lyu, L. Bai, and X. Huang, “Real-time road segmentation using lidar data processing on an fpga,” in *2018 IEEE International Symposium on Circuits and Systems (ISCAS)*. IEEE, 2018, pp. 1–5.
- [32] —, “Chipnet: Real-time lidar processing for drivable region segmentation on an fpga,” *IEEE Transactions on Circuits and Systems I: Regular Papers*, vol. 66, no. 5, pp. 1769–1779, 2018.
- [33] S. Liu and W. Luk, “Towards an efficient accelerator for dnn-based remote sensing image segmentation on fpgas,” in *2019 29th International Conference on Field Programmable Logic and Applications (FPL)*. IEEE, 2019, pp. 187–193.
- [34] L. Bai, Y. Lyu, and X. Huang, “A unified hardware architecture for convolutions and deconvolutions in cnn,” in *2020 IEEE International Symposium on Circuits and Systems (ISCAS)*. IEEE, 2020, pp. 1–5.
- [35] J. Shen, D. Wang, Y. Huang, M. Wen, and C. Zhang, “Scale-out acceleration for 3d cnn-based lung nodule segmentation on a multi-fpga system,” in *Proceedings of the 56th Annual Design Automation Conference 2019*, 2019, pp. 1–6.
- [36] K. He, X. Zhang, S. Ren, and J. Sun, “Deep residual learning for image recognition,” in *Proceedings of the IEEE conference on computer vision and pattern recognition*, 2016, pp. 770–778.
- [37] X. Glorot and Y. Bengio, “Understanding the difficulty of training deep feedforward neural networks,” in *Proceedings of the thirteenth international conference on artificial intelligence and statistics*, 2010, pp. 249–256.
- [38] L. Sifre and S. Mallat, “Rigid-motion scattering for image classification, 2014,” Ph.D. dissertation, Ph. D. thesis, 2014.
- [39] F. Chollet, “Xception: Deep learning with depthwise separable convolutions,” in *Proceedings of the IEEE conference on computer vision and pattern recognition*, 2017, pp. 1251–1258.
- [40] A. G. Howard, M. Zhu, B. Chen, D. Kalenichenko, W. Wang, T. Weyand, M. Andreetto, and H. Adam, “Mobilenets: Efficient convolutional neural networks for mobile vision applications,” *arXiv preprint arXiv:1704.04861*, 2017.
- [41] M. Sandler, A. Howard, M. Zhu, A. Zhmoginov, and L.-C. Chen, “Mobilenetv2: Inverted residuals and linear bottlenecks,” in *Proceedings of the IEEE Conference on Computer Vision and Pattern Recognition*, 2018, pp. 4510–4520.
- [42] F. Yu and V. Koltun, “Multi-scale context aggregation by dilated convolutions,” *arXiv preprint arXiv:1511.07122*, 2015.
- [43] C. R. Qi, H. Su, K. Mo, and L. J. Guibas, “Pointnet: Deep learning on point sets for 3d classification and segmentation,” in *Proceedings of the IEEE conference on computer vision and pattern recognition*, 2017, pp. 652–660.
- [44] *BatchNorm after ReLU*, 2016 (accessed May 3, 2020). [Online]. Available: <https://github.com/gcr/torch-residual-networks/issues/5>
- [45] “Qkeras: a quantization deep learning library for keras,” <https://github.com/google/qkeras>, accessed: 2019-12-06.
- [46] Y. Fu, E. Wu, A. Sirasao, A. Attia, K. Khan, and R. Wittig, “Deep learning with int8 optimization on xilinx devices,” *White Paper WP486, Xilinx*, 2017.
- [47] OpenCV, “Open source computer vision library,” 2015.
- [48] C. C. T. Mendes, V. Frémont, and D. F. Wolf, “Exploiting fully convolutional neural networks for fast road detection,” in *2016 IEEE International Conference on Robotics and Automation (ICRA)*. IEEE, 2016, pp. 3174–3179.
- [49] S. Zhang, Z. Zhang, L. Sun, and W. Qin, “One for all: A mutual enhancement method for object detection and semantic segmentation,” *Applied Sciences*, vol. 10, no. 1, p. 13, 2020.
- [50] F. A. Reis, R. Almeida, E. Kijak, S. Malinowski, S. J. F. Guimarães, and Z. K. do Patrocínio, “Combining convolutional side-outputs for road image segmentation,” in *2019 International Joint Conference on Neural Networks (IJCNN)*. IEEE, 2019, pp. 1–8.
- [51] R. Fan, Y. Wang, L. Qiao, R. Yao, P. Han, W. Zhang, I. Pitas, and M. Liu, “Pt-resnet: Perspective transformation-based residual network for semantic road image segmentation,” *arXiv preprint arXiv:1910.13055*, 2019.
- [52] D. Levi, N. Garnett, E. Fetaya, and I. Herizlyia, “Stixelnet: A deep convolutional network for obstacle detection and road segmentation,” in *BMVC*, 2015, pp. 109–1.
- [53] T. Kühnl, F. Kummert, and J. Fritsch, “Spatial ray features for real-time ego-lane extraction,” in *2012 15th International IEEE Conference on Intelligent Transportation Systems*. IEEE, 2012, pp. 288–293.
- [54] M. Oeljeklaus, F. Hoffmann, and T. Bertram, “A fast multi-task cnn for spatial understanding of traffic scenes,” in *2018 21st International Conference on Intelligent Transportation Systems (ITSC)*. IEEE, 2018, pp. 2825–2830.
- [55] M. Passani, J. J. Yebe, and L. M. Bergasa, “Fast pixelwise road inference based on uniformly reweighted belief propagation,” in *2015 IEEE Intelligent Vehicles Symposium (IV)*. IEEE, 2015, pp. 519–524.
- [56] L. Xiao, B. Dai, D. Liu, D. Zhao, and T. Wu, “Monocular road detection using structured random forest,” *International Journal of Advanced Robotic Systems*, vol. 13, no. 3, p. 101, 2016.
- [57] M. Passani, J. J. Yebe, and L. M. Bergasa, “Crf-based semantic labeling in miniaturized road scenes,” in *17th International IEEE Conference on Intelligent Transportation Systems (ITSC)*. IEEE, 2014, pp. 1902–1903.
- [58] J. M. Alvarez, T. Gevers, Y. LeCun, and A. M. Lopez, “Road scene segmentation from a single image,” in *European Conference on Computer Vision*. Springer, 2012, pp. 376–389.